remote sensing

MDPI

Article

Vegetation Height Estimate in Rice Fields Using Single Polarization TanDEM-X Science Phase Data

Seung-Kuk Lee [1,2], Sun Yong Yoon [3] and Joong-Sun Won [3,*]

[1] Biospheric Sciences Laboratory, National Aeronautics and Space Administration/Goddard Space Flight Center, Greenbelt, MD 20771, USA; seungkuk.lee@nasa.gov
[2] Department of Geographical Sciences, University of Maryland, College Park, MD 20742, USA; sklee@umd.edu
[3] Department of Earth System Sciences, Yonsei University, Seoul 03722, Korea; yoonsy42@yonsei.ac.kr
* Correspondence: jswon@yonsei.ac.kr; Tel.: +82-2123-2673

Received: 18 September 2018; Accepted: 26 October 2018; Published: 29 October 2018

Abstract: This study presents the retrieval of rice paddy height using single polarization (single-pol) interferometric SAR (InSAR) data by means of model-based height inversion without an external DEM. A total of eight TanDEM-X (TDX) scenes were used and the TDX images were; acquired using a large cross-track baseline configuration during the TDX Science Phase (June–August 2015). A single-pol inversion approach for a flooded rice field is proposed and evaluated over the Buan test site in South Korea. A novel approach is adopted for the estimation of the ground (i.e., water level) interferometric phase within a flooded rice paddy from TDX data acquired during a period of early rice growth. It is consequently possible to apply the model-based inversion algorithm to the single-pol InSAR data. Rice height maps during the rice growth cycle presented and validated by field measurements. The results demonstrated the high performance of the inversion with a correlation coefficient of 0.78 and an RMSE of 0.10 m. The proposed methodology will be useful to monitor rice plants and to predict a gross rice yield, along with dual and fully polarimetric interferometric SAR data.

Keywords: rice paddy height; single-pol InSAR; height inversion; TanDEM-X; TDX science phase

1. Introduction

Rice is a major food crop and is the most widely consumed for a large part of the world's human population, especially in Asia. Asia accounts for more than 90 percent of world rice production and consumption and is important for the food security of approximately half of the world's population. Global rice consumption has increased by a factor of three since the 1960's from 150 million tons to 450 million tons per year [1]. Rice is also a strategic commodity as the overall economic growth and political stability of the region depend on an adequate, cheap, and stable supply of this staple crop [2]. Therefore, it is important to forecast and estimate annual rice production using a method of rice growth efficiently, over large geographical areas.

The height of vegetation is one key factor used when assessing a potential crop yield. Traditionally crop heights have been estimated through field inventory assessments. This, however, is expensive, time consuming, staff intensive, and yields discrete point-based measurements. Remote sensing approaches have attempted to provide an alternative for crop growth monitoring. Airborne lidar is the most accurate method for estimating vegetation height but is limited by its cost over large geographical areas and data volume required to monitor a long-term change (or growth) in the vegetated area of interest.

Polarimetric SAR interferometry (Pol-InSAR) is a well-known technique for the retrieval of 3-D forest structural parameters [3], through the coherent combination of both polarimetric and interferometric observables, providing a step forward in quantitative 3-D forest parameter estimation [3–6]. Several airborne SAR experiments first demonstrated the potential of Pol-InSAR techniques at multi-frequencies to estimate key forest structure parameters with a high vertical accuracy [7–12]. Recent studies have demonstrated the retrieval of forest parameters using Pol-InSAR techniques with spaceborne data [13]. The quality of the retrieved heights by means of InSAR and Pol-InSAR applications critically depends on non-volumetric decorrelation contributions (cf. volume decorrelation is directly related to forest structure in the height inversion) and the height sensitivity defined by the spatial baseline and wavelength of the radar signal [14]. Amongst non-volumetric decorrelation contributions, the most critical factor is temporal decorrelation caused by changes in the scatterers in terms of a conventional airborne/spaceborne repeat-pass system [8,11,14]. Several studies determined and mitigated the effect of temporal decorrelation using airborne data gathered with a narrow temporal baseline [8,11]. Traditional spaceborne SAR missions operated by a single satellite had revisit times too long to avoid strong temporal decorrelation effects in forest height inversion. In addition to temporal decorrelation, the distance between the positions of the radar sensor is also a key parameter that scales the height sensitivity for model-based inversions and determines the available height range possible to invert [6,9,15].

TanDEM-X (TDX: TerraSAR add-on for digital elevation measurements) is the first single-pass interferometer with an X-band wavelength within a unique flying formation of two satellites that eliminates the effects of any temporal decorrelation [16,17]. The TDX mission successfully generated a consistent global digital elevation (DEM) model at 12-m and 30-m spatial resolution with an unprecedented vertical accuracy [18,19]. Beyond the main objective of global DEM generation, TDX has been the first to demonstrate vegetation parameter estimates over a variety of forest types (tropical, temperate, and boreal areas) from space [13,15,20–24]. In addition to estimating forest structural parameters, the potential of TDX images for monitoring biophysical variables in rice paddies was evaluated from a stack of 16 dual-pol TDX images acquired in 2012 and 2013 (i.e., TDX DEM mission period) with a height ambiguity from 23.1 m to 52.8 m [25]. During the TDX mission period, the spatial baseline between 200 m and 300 m was designed for the generation of global X-band DEM. This spatial baseline is well-suited to estimate the top canopy forest height, but is too short to measure crop height as small residual non-volumetric decorrelations cause large height errors, especially for short vegetation in model-based height inversion.

Beyond the primary TDX mission goal, the TDX Science Phase was completed to demonstrate innovative techniques and experiments with special orbital and imaging requirements from October 2014 to December 2015 [26,27]. Fortunately, during the TDX Science Phase, some TDX data sets were acquired using a large cross-track baseline of 3–4 km. This provided an opportunity to generate crop height maps and analyze the temporal trend of crop height using satellite data with large-coverage and regular revisit time. Pol-InSAR based crop height estimations were first performed using TDX image acquired by dual-pol mode in September 2015 [28]. The evaluation of changes in rice height through time has recently been published using a Pol-InSAR inversion technique with dual-pol TDX Science Phase datasets [29]. The estimation of rice height using Pol-InSAR inversion was tested over test sites in Spain and Turkey with different rice varieties and over the whole cultivation campaign, from sowing to plant maturity. In [30], dual-pol inversion results were combined with stochastic inversion algorithms for small-scaled morphological changes for the complete growth cycle of rice plant. However, in order to obtain dual-pol data in the TDX antenna system, two polarizations are required by toggling the polarization from pulse to pulse, resulting in lower spatial resolution or narrower swath, compared to single-pol TDX data [31]. This limits the image resolution or coverage that can be imaged by TDX compared to a single-pol case. Recent study showed a first work with an example of rice height retrieval at the end of the growth cycle from single-pol TDX data sets over South Korea [32].

This paper is aimed at evaluating the retrieval of rice paddy height for a complete growth cycle from post-transplanting to maturation stage by means of single-pol TDX Science Phase data sets. We use a total of eight InSAR acquisitions from 12 June to 28 August 2015, with an 11-day time interval. Here, we utilize the single-pol height inversion approach based on the algorithm described in [15,20] to solve underdetermined components in the random volume over ground (RVoG) model from single polarization InSAR data. The traditional method for cultivating rice is through flooding the paddy during or after, sowing the young rice seedling. We assume that the underlying topography is completely flat in flooded fields. For crop height inversion above the flooded water surface, the water level estimate in rice paddies during the early stage of rice growth made the single-pol inversion possible without another polarization channel or an external topography information. In Section 2 the test site, TDX Science Phase data, and in-situ measurement data are introduced. Section 3 briefly reviews the Pol-InSAR inversion using not only quad-pol but also single-pol InSAR data. And, the water level estimate in the rice paddy is proposed and investigated only using TDX Science Phase data acquired during the early stage of the rice growth cycle. Section 4 demonstrates the validation of the estimated rice height by means of the single-pol inversion approach. Finally, the discussion and conclusion are presented in the last section.

2. Data Sets and Test Site

2.1. TDX Data Sets & InSAR Processing

The TDX data used in this study were acquired during the large baseline bistatic configuration of the TDX Science Phase. In the frame work of the German Aerospace Center (DLR) project *XTI_OCEA6660*, a total of eight single-pol (HH) TDX pairs were continuously acquired over Buan, South Korea with a revisit time of 11-days, from 12 June 2015 (DoY-162) to 28 August 2015 (DoY-261) (see Table 1). The distance between two TDX satellites increased up to three–four km in order to reduce the height of the ambiguity (HoA) for short vegetation application. The HoA of all acquisitions was ~3.14 m. The polarization was HH and the system bandwidth was 150 MHz.

The TDX data sets were acquired in bistatic mode: one satellite acts as a transmitter and both satellites simultaneously receive the signal backscattered by the earth's surface. Subsequently, temporal decorrelation effects do not exist in the height inversion. The SAR data were provided in the Coregistered single-look slant-range complex (CoSSC) format from DLR [33]. We measured interferometric complex coherence with ~50 looks to fix the postspacing at 20 m. Range spectral filtering was implemented to compensate for geometric range decorrelation caused by a non-common spectrum, especially prominent at a large spatial baseline. The large baseline used in this study led to subsequent shifts in the wavenumber, reaching 37.30 MHz [34,35]. In order to stack the measured interferometric phases, the absolute phase calibration was performed using Shuttle Radar Topography Mission (SRTM) data [25].

Table 1. List of TDX image pairs over Buan test sites.

Date (yyyy/mm/dd)	DoY [1] [days]	Incidence Angle [Deg.]	Polarization	*kz* [Rad/m]	Height of Ambiguity [m]
2015/06/12	162	28.98	HH	−2.00	−3.14
2015/06/23	173	28.98	HH	−2.00	−3.14
2015/07/04	184	28.98	HH	−2.00	−3.14
2015/07/15	195	28.98	HH	−2.00	−3.14
2015/07/26	206	28.98	HH	−2.00	−3.14
2015/08/06	217	28.98	HH	−2.00	−3.14
2015/08/17	228	28.98	HH	−2.00	−3.14
2015/08/28	239	28.98	HH	−2.00	−3.14

[1] DoY: Day of Year from 1 January 2015.

2.2. Test Site and In-Situ Data

The study area of Buan is located on the West coast of South Korea (see Figure 1). In South Korea, 50.7% of cultivated land area was used for growing rice in 2015 [36]. Although rice consumption in South Korea has gradually decreased, it remains the largest source of calorie intake. Rice paddies in South Korea are divided into rectangular shaped parcels with an extent of ~0.5 ha (~50 m × ~100 m). Rice paddies in the TDX imagery cover an area of ~5 km × ~5 km over a total of 3515 parcels. Location of each parcel is provided within Digital Topography Map (DToM) data from National Geographic Information Institute (NGII) for South Korea. It provides Geographic Information System (GIS) datasets in a shape file format. We used the farmland layer of the DToM with a scale of 1:5000 to distinguish rice paddy parcels, as shown in Figure 2.

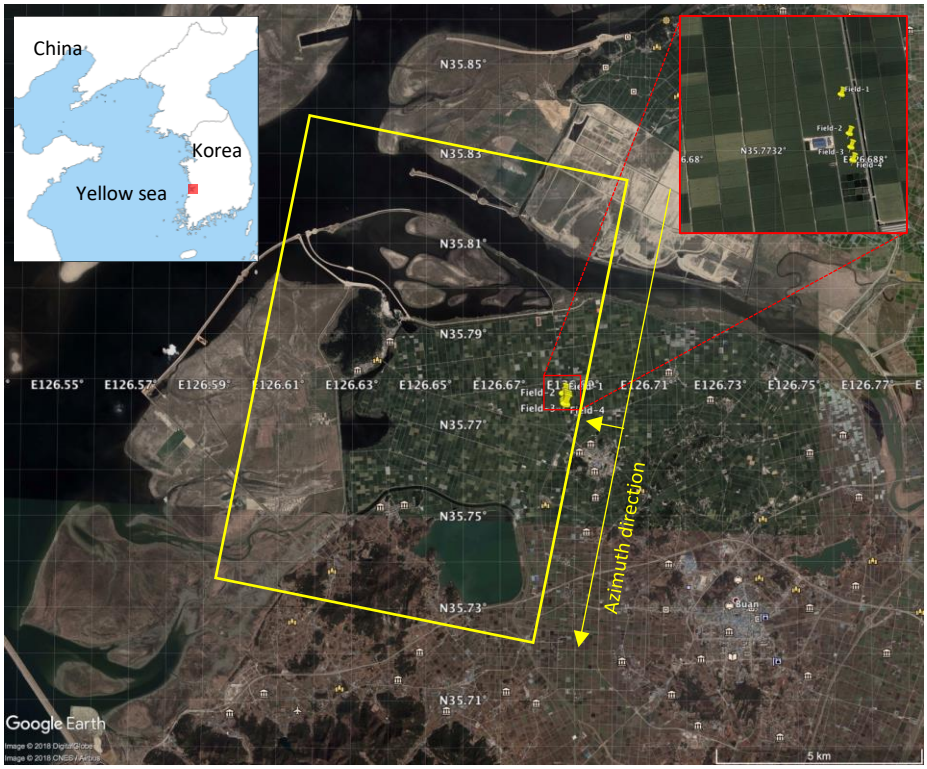

Figure 1. Location of the Buan test site. Data source: Google Earth. 29 August 2015. Pins show location of parcels for field measurement. Yellow rectangle shows the frame of TDX image for the study area.

The rice growth cycle in South Korea from sowing to plant maturity occurs over a period of 120–180 days. Rice plants were sown at points in regular straight lines with a density of three–four rice seedlings per point. The distance between points along a line was ~15 cm with a distance between lines of ~30 cm, covering 20–25 seedling points per one square meter (see Figure 2). The planting period occurred from early May to mid-June. The rice paddy is flooded to a depth of ~10 cm both prior to and following planting.

In-situ measurements of rice height at four rice paddies were recorded at the Buan test site by the National Institute of Agricultural Sciences (NAAS). Ground truth data for rice height during the TDX science phase period in 2015 were provided by NAAS, and are listed in Table 2. It is important to note that the height measured by NAAS is the height from the rice root to the top of the plant after rooting out, whilst the inversion height measures the height of the bent plant from the paddy water surface. To estimate these differences in measurement method, both heights were measured in 2017 and are shown in Figure 3. The average difference between the two heights was 10.5 cm with a standard deviation of 3.8 cm.

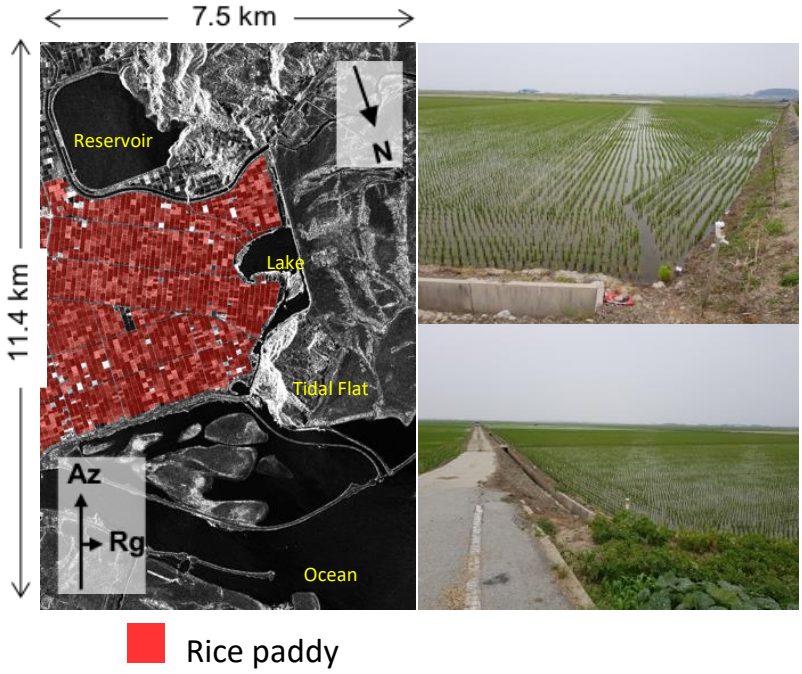

Figure 2. Region of interest within the Digital Topography Map (DToM) is overlain on the TDX amplitude image. Photographs show rice fields in the test site taken on 10 June 2017.

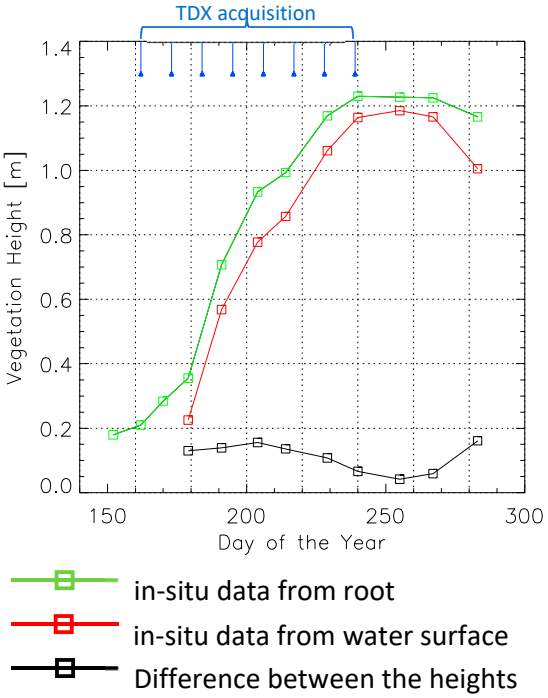

Figure 3. The relationship between the day of the year (DoY) and the rice height. Rectangle represents field measurement date. Green: Entire vegetation height from root to top after rooting out. Red: Top canopy height above the water surface. Black: Difference between the heights on the DoY.

Table 2. Field measurement data.

Date (yyyy/mm/dd)	DoY [1] [days]	Field-1 [m]	Field-2 [m]	Field-3 [m]	Field-4 [m]
2015/05/29	148	18.9	16.9	18.4	16.2
2015/06/09	159	25.5	24.1	23.7	27.5
2015/06/24	174	42.0	41.4	38.9	35.2
2015/07/10	190	51.8	57.3	65.6	62.9
2015/07/20	200	75.7	83.4	83.3	81.6
2015/08/06	217	89.4	92.8	95.4	93.7
2015/08/20	231	108.1	110.9	116.6	107.0
2015/09/04	246	104.1	107.9	115.4	116.6
2015/09/19	261	108.6	110.5	118.8	112.0
2015/10/06	278	105.1	106.3	116.4	109.0

[1] DoY: Day of Year from 1 January 2015.

3. Methodology

3.1. Single-Pol InSAR Height Inversion Approach

Pol-InSAR is a well-known advanced radar technique for retrieving the 3-D parameters of vegetation structure, which makes use of the coherent combination of polarimetric and interferometric observables to separate different scattering centers of the polarization from underlying topography to the vegetation canopy. In the last decade, the Pol-InSAR based canopy height estimation has been used to determine the height of various types of forested area. Most inversion approaches have employed the Random Volume over Ground (RVoG) model that is a widely and successfully used model for the retrieval of the parameters of 3-D vegetation [5–7]. The model has a realistic scattering mechanism for vegetated scenes formed by volume and ground layers. The vertical reflectivity fusion $F(z)$ in the two-layered model is coherently modeled as a volume layer of a thickness h_V containing randomly oriented particles described by a vertical scattering function and an impenetrable ground layer at $z = z_0$. The interferometric coherence $\widetilde{\gamma}(\kappa_z;\vec{\omega})$ at a polarization $\vec{\omega}$ in a vegetated area is a function of the vertical interferometric wavenumber κ_z and can be described as

$$\widetilde{\gamma}(\kappa_z;\vec{\omega}) = e^{i\phi_0}\frac{\int_0^{h_V} F(z)e^{i\kappa_z z}dz}{\int_0^{h_V} F(z)dz} = e^{i\phi_0}\frac{\widetilde{\gamma}_V(h_V,\sigma;\kappa_z,\theta_0)+\mu(\vec{\omega})}{1+\mu(\vec{\omega})} \quad (1)$$

with

$$\kappa_z = m\frac{2\pi}{\lambda}\frac{\Delta\theta}{sin\theta_0} = \frac{2\pi}{h_{2\pi}} \quad (2)$$

where ϕ_0 is the ground phase related to the elevation of the ground layer ($\phi_0 = \kappa_z z_0$). A mean extinction σ expresses the sum of scattering and absorption and $\mu(\vec{\omega})$ represents the effective ground-to-volume amplitude ratio at a polarization. The factor m in the vertical wavenumber κ_z depends on interferometric acquisition mode: m = 2 for the monostatic case and m = 1 for the bistatic case (e.g., TDX single-pass interferometric mode). The angle difference $\Delta\theta$ is between master and slave ranges and $h_{2\pi}$ is the height of the ambiguity in radar interferometry and the maximum height possible to estimate forest height inversion. Equation (1) can be solved with fully polarimetric (or at least dual-polarimetric) interferometric data with an assumption of no response from the ground in one polarization, but in case of single-pol acquisition, the inversion is unbalanced with the three unknowns (h_V, σ, and ϕ_0) in the two-layer model.

To solve the underdetermined problem in single-pol inversion, an external DTM was used to estimate the ground phase in order to reduce one unknown parameter in the RVoG model [7,13,21–24]. Over mangrove forests, a recent single-pol TDX approach eliminated the underlying topography by using the water surface (i.e., ground phase ϕ_0 in the RVoG model) directly from the boundary of the mangrove forest and adjacent water body using the assumption of a flooded and subsequent

flat topography [15,20]. In this study, we here suggest to estimate the ground (water) phase directly from the TDX interferogram acquired during the early stage of the rice growth cycle. For this, it was assumed that the water surface within each rice paddy parcel is completely flat.

3.2. Ground Phase Estimation on Rice Paddy

Recent studies have investigated the physical interaction between the radar signal and rice paddy setting [25,28,29,37–44]. Before the planting of the rice seedling into fields, they are covered by water and the rice plant grows beneath a flooded surface. The rice fields are separated by a path network composed by soil or cement roads (See Figure 2). The water surface behaves like mirror to incident radar energy, reflecting the transmitted radar signal in a specular direction, yielding very low returns of the signal to SAR antenna. In this case, a low interferometric coherence is obtained and the quality of the interferogram is significantly poor, yielding unreliable water level elevation values. During the early state of rice growth, the rice plant is not dense enough to cover the rice paddy and gaps exist between adjacent plants. A double-bounce scattering mechanism is generated by the interaction between the rice plants and the open water surface, yielding strong radar signal returns. The double-bounce radar scattering mechanism is the two-bounce travel path of the radar pulse and it is equal to the one-bounce travel path on the water surface (or on the bottom of the rice stem) [45,46]. Therefore, the interferometric phases with double-bounce scattering mechanism represents the ground (i.e., water surface) level elevation during the early stage of rice growth.

The TDX amplitude and coherence images over the test site from 12 June to 28 August 2015 are shown in Figures 4 and 5. In the first TDX acquisition (12 June 2015), the radar backscattering coefficient varied strongly parcel by parcel, in relation to the transplanting time managed by the field owner. Consequently, three scenarios of rice paddy cover occurred and needed to be considered separately to achieve the ground phase estimate. These cover conditions were (1) a rice plant of a given height after post-transplanting, (2) a water surface immediately post-transplanting, and (3) a bare surface. The transplanting of rice seedlings into a field occurred prior to a small number of weeks and the plants reached a height sufficient enough to cause an interaction between the radar signal and the water surface. This caused a strong backscattering power and high coherence, yielding a reliable elevation estimate. However, in rice fields covered by water with no plant or rice seedlings, the transmitted radar signal was not returned to the radar antenna, resulting in a low interferometric coherence due to the strong SNR decorrelation. In this case, we estimated the ground phase using a parcel from the next (second or third) acquisition of TDX imagery that behaved like the first scenario case. Lastly, for parcels with a bare surface (no water and no plant), a wet and rough soil surface yielded a strong return to the SAR antenna and a high coherence was achieved in the first acquisition (see tidal flat areas in Figure 4). However, on the second acquisition, the radar signal and the interferometric coherence decreased rapidly due to the flooding for the rice seedling. In this case, we took the interferometric phases from the third acquisition (4 July 2015) of the TDX data, if coherence values were sufficient to reliably measure the water level elevation. In order to estimate the ground phase over the entire test site, we continuously used three TDX images from the first acquisition date. The ground phase of 69.4% of parcels were measured from the TDX interferogram on the second date (23 June 2015). The first and third acquisitions of TDX were used to estimate the water level within parcels accounting for 3.0% and 24.8% of the parcels, respectively. Unfortunately, 2.8% of parcels demonstrated low signal returns and low coherence values by the third acquisition and were excluded. The ground phase was finally measured using the mode value of the interferometric phases selected by a coherence value higher than 0.95 on a parcel-by-parcel basis. The ambiguity of the ground phase estimate increased with rice growth due to a stronger volume contribution, yielding an overestimation of water level. Hence, we only used the first three acquisitions for the ground phase estimation within the rice paddies.

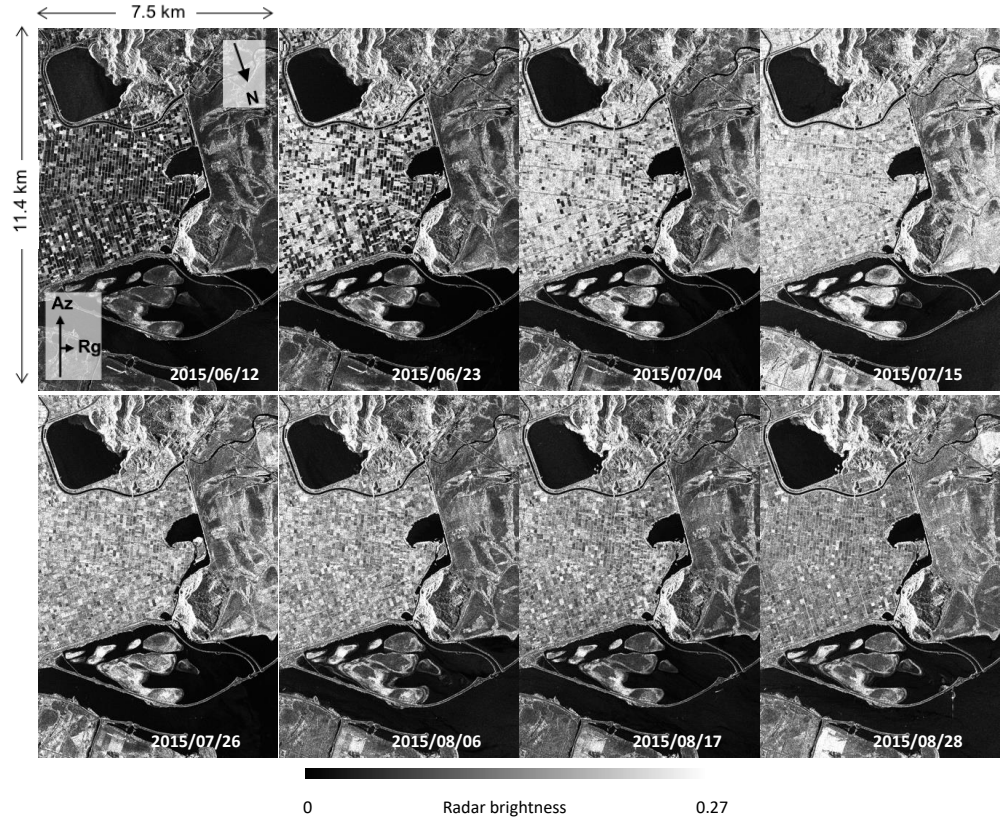

Figure 4. Amplitude images at HH polarization of TDX from 12 June to 28 August 2015.

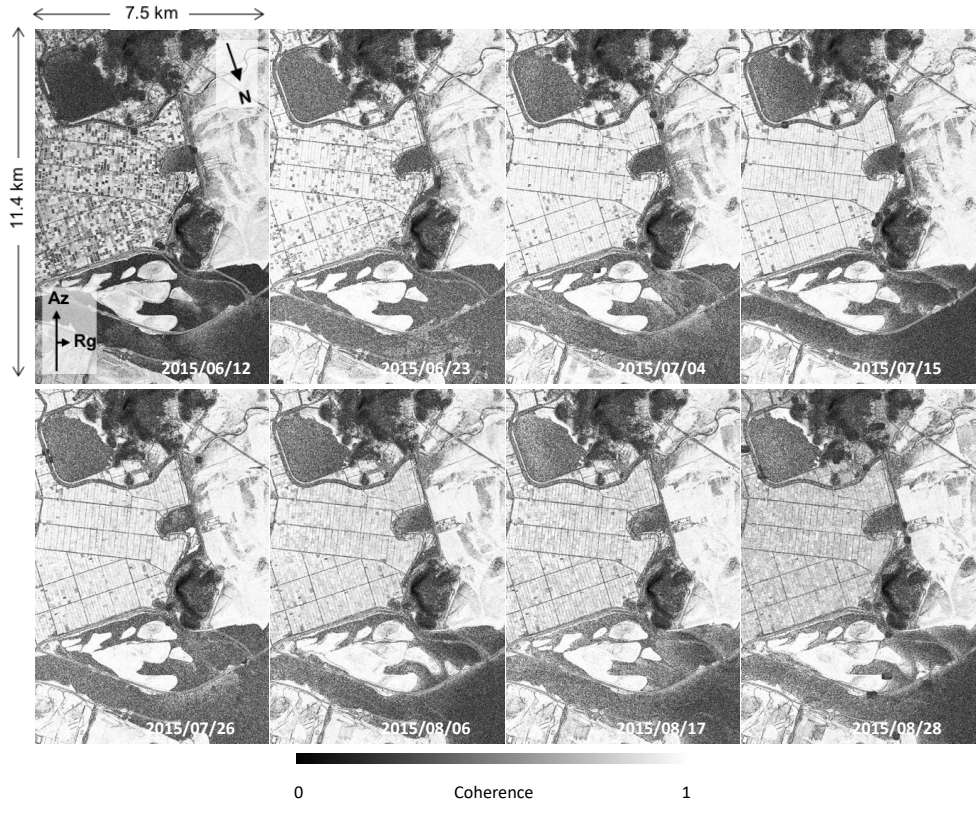

Figure 5. Coherence images at HH polarization of TDX, scaled from 0 (black) to 1 (white), from 12 June to 28 August 2015.

3.3. Inversion

Refining volume coherence from non-volumetric decorrelation contributions is an important step in Pol-InSAR inversion. In a repeat-pass InSAR system, temporal decorrelation has an adverse impact on height estimation, but the effects of temporal decorrelation can be ignored in this case due to the bistatic mode of the TDX mission. However, the large spatial baseline of the TDX Science Phase datasets used results in shifts in the wavenumber. It is, therefore, essential to apply range spectral filtering to all TDX data acquired with a large spatial baseline. After the compensation for range decorrelation, the effect of the signal-to-noise ratio (SNR) has to be compensated for a pure volume-only decorrelation estimate. The SNR decorrelation $\widetilde{\gamma}_V$ is one of the main decorrelation contributions for TDX [16] and it is introduced by the finite sensitivity of each TDX receiver. It can be a real number and described for the two satellites of the TDX mission as

$$\widetilde{\gamma}_{SNR} = \frac{1}{\sqrt{(1 + SNR_{TSX}^{-1})(1 + SNR_{TDX}^{-1})}} \tag{3}$$

where $SNR_{\{TSX,TDX\}}$ are the SNR for each interferometric channel of TSX and TDX for a given polarization. The exact SNR depends primarily on the strength of the returned signal and it can be described by the ratio of the normalized backscattering coefficient σ_0 and the noise equivalent sigma zero (NESZ). The NESZ of TDX can be computed from the annotated values of NESZ patterns provided in the standard TDX products [16,20,47]. The SNR decorrelation of TDX depends on the polarimetric channel (HH, HV, VH, and VV), polarimetric mode (SRA and DRA), imaging mode (SM, HS, and SC), and so on [31].

Once volume-only coherence and the ground phase (ϕ_0) estimate have been obtained, we could apply the single-pol inversion approach for estimating rice height within the rice paddies. The inversion is based on the method of the minimum distance between the compensated TDX volume coherence $\widetilde{\gamma}(\vec{\omega})$ and the look-up table (LUT) of the modelled coherences $[\widetilde{\gamma}_V e^{i\phi_0}]$ [20]:

$$\min_{h_V,\sigma,\phi_0} \| [\widetilde{\gamma}(\vec{\omega})] - [\widetilde{\gamma}_V e^{i\phi_0}] \| \tag{4}$$

Note that the single-pol inversion approach is not based on the traditional Pol-InSAR method of the line fit to estimate the underlying topography (i.e., the ground phase) and to define the coherence with minimum ground contribution (i.e., volume-only coherence) for dual or fully polarimetric interferometric data [5,7–9,29].

4. Results

This section presents the sequential backscattered power and interferometric volume coherence for all TDX acquisitions in the four parcels, with the available field measurement mentioned in the Section 2.2 (Figure 6). At the first date, TDX amplitudes are very low, since rice seedlings were recently planted into a flooded field or because the field was ready for transplanting. Consequently, the interferometric coherences are too low to get reliable ground phase information from the water surface because the SNR decorrelation dominates the measured TDX coherences, yielding inaccurate phase estimates. On the second acquisition date, the amplitude power increases dramatically and is much stronger, resulting in the highest coherence level for all parcels. This is interpreted as double-bounce scattering between the rice plants and the water surface in the fields. From the third date, the coherence decreases slowly with a monotonically increasing trend of rice growth until the plants late reproductive stage, leading to more volumetric decorrelation contributions in the measured interferometric coherence. At the last two acquisition dates, the volume coherence starts decreasing steeply to approximately 0.80 on the last date.

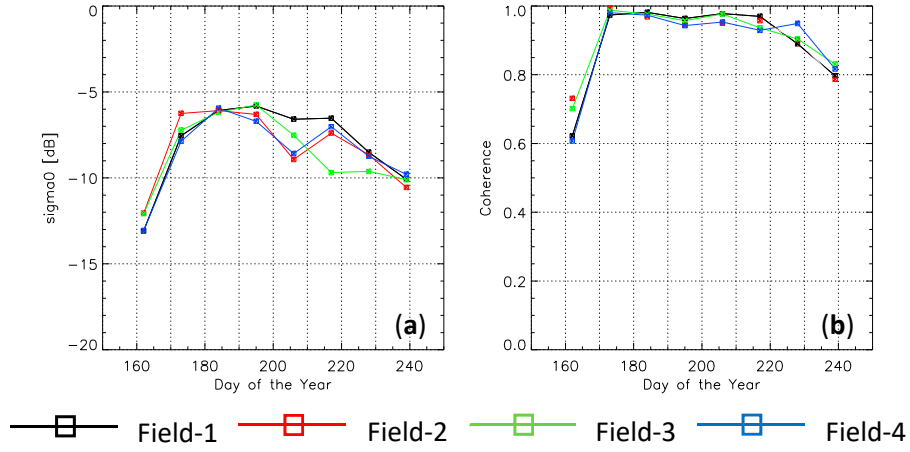

Figure 6. Temporal variation of TDX sigma nought (**a**) and coherence (**b**) in the inventory fields.

For the rice height inversion, the ground phase for all parcels of the field campaign was measured using the second acquisition, making the height inversion possible from the third TDX acquisition (4 July 2015) to the last date (28 August 2015). Figure 7 shows the successive growth of the rice through the inversion height. Each plot shows in-situ data (green) and the height estimation from TDX (black) in different fields. For all parcels, the inverted heights are lower than the ground data from DoY-206 to DoY-239. As mentioned in the Section 2.2, the in-situ height is traditionally defined as the plant height from root to top after rooting out, whereas the inversion height represents the top canopy height of the vegetation from the water surface. In order to properly analyze the two different vegetation heights, the in-situ data in 2015 was modified to the top canopy height above the water surface using the change in water level during a rice growth cycle in 2017 (Figure 3). Red lines in Figure 7 represent the modified rice height within each parcel. The retrieved vegetation heights between TDX and the ground data become closer to the field measured height after compensating the water depth, whereas the first inversion results (DoY-184) for all parcels are overestimated and the height error reaches ~20%. Although the TDX Science Phase data was acquired using a very large spatial baseline (HoA of ~3.14 m), the InSAR acquisition still suffers due to a lack of interferometric sensitivity for very short vegetation (<0.5 m). In this case, small residual non-volumetric decorrelation causes large height errors, estimated at more than 20% of inversion error. In the case of very short vegetation, the spatial baseline should be much longer than the one used in this study. Although the inversion results are over or under-estimated from DoY-195, depending on the parcel and the date, the heights estimated correspond well with the rice growth measured.

Figure 8 visually shows the rice plant growth using the inversion heights over a large area of the Buan test site from 23 June to 28 August 2015. We estimated the ground phase parcel by parcel from the first TDX acquisition on 12 June 2015, but only 104 parcels (3.0%) showed a reliable water level measurement, enabling the retrieval of rice heights using the estimated ground phase on the second acquisition date. On the second and third dates, we could additionally measure the ground phase in parcels accounting for 2440 and 870 of parcels, respectively. The coverage of the vegetation height mapped on the third date reaches 72.4% of the rice paddy test site. From the fourth date onwards, the single-pol inversion is applied to 97.2% of parcels in a large rice paddy area, whereas 2.8% of parcels were excluded from the height inversion due to the retrieval of an unreliable elevation estimate caused by a low coherence level until the third acquisition. From these maps, we could monitor the growth trend within each parcel over the test site. The map of the rice paddy height in late August shows the growth of the plants, reaching up to ~1 m, twice as large compared to heights in June. The time-series height information will be useful for agricultural planning, vegetation growth monitoring and natural hazard vulnerability (typhoon, drought, and insect) and its implications upon final rice production.

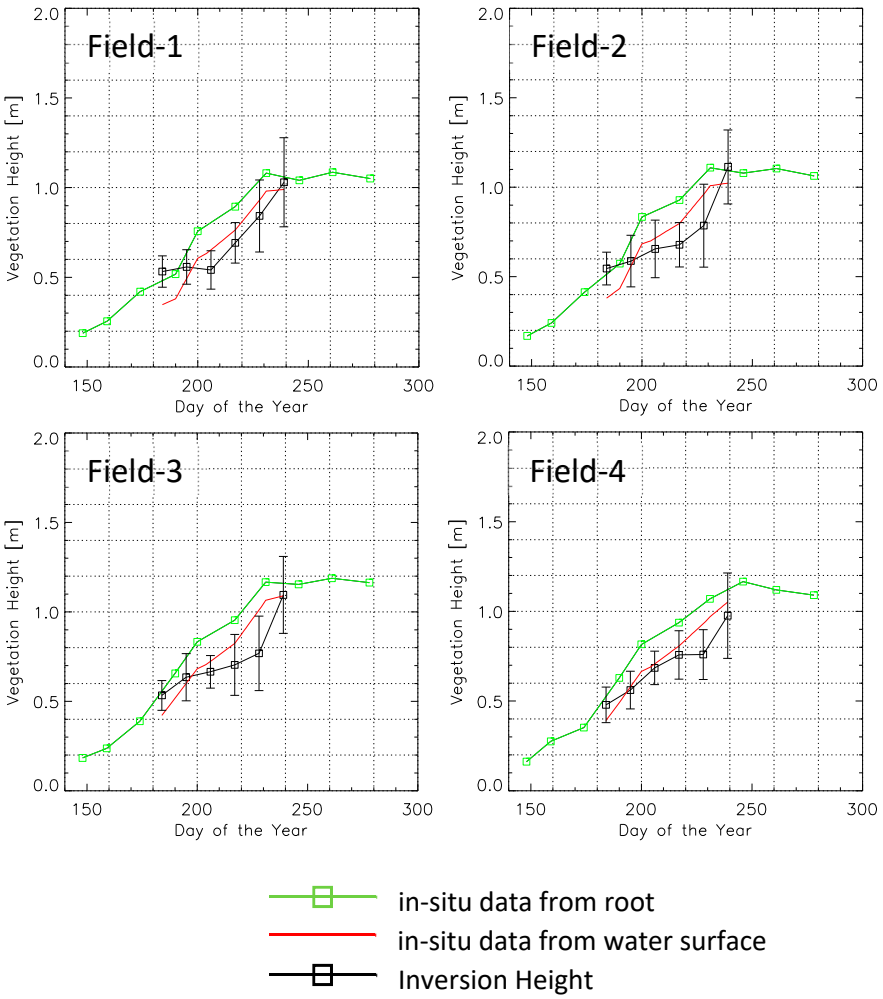

Figure 7. Mean temporal TDX rice height trend for the inventory fields (black line). The standard deviation is highlighted with error bars. The reference heights are overplotted with colors. Green line shows field measurement of root-to-top and red line is a field rice height above water surface.

The validation plots between the TDX inversion height and the in-situ measurements are shown in Figure 9. In order to quantitatively compare the heights, we plot the average inversion height in each parcel over all dates, against two different ground data sets provided by the field campaign. The comparison between the inversion results and the in-situ rice height from root to top is displayed in Figure 9a. In Figure 9b, the retrieved heights are plotted against the field rice height data from water surface to rice canopy. The validation of the rice height from water surface demonstrates the high performance of the single-pol inversion with a correlation coefficient R^2 of 0.78 and an RMSE of 0.10 m. The comparison of the TDX inversion height and the entire vegetation height from the root is characterized by an R^2 of 0.72 and an RMSE of 0.18 m. Although the inversion result on rice height shorter than 0.50 m shows a larger height error, the overall estimation accuracy for the rice paddy height from 0.38 m to 1.08 m is better than 10% for the single-pol TDX inversion approach proposed in the study.

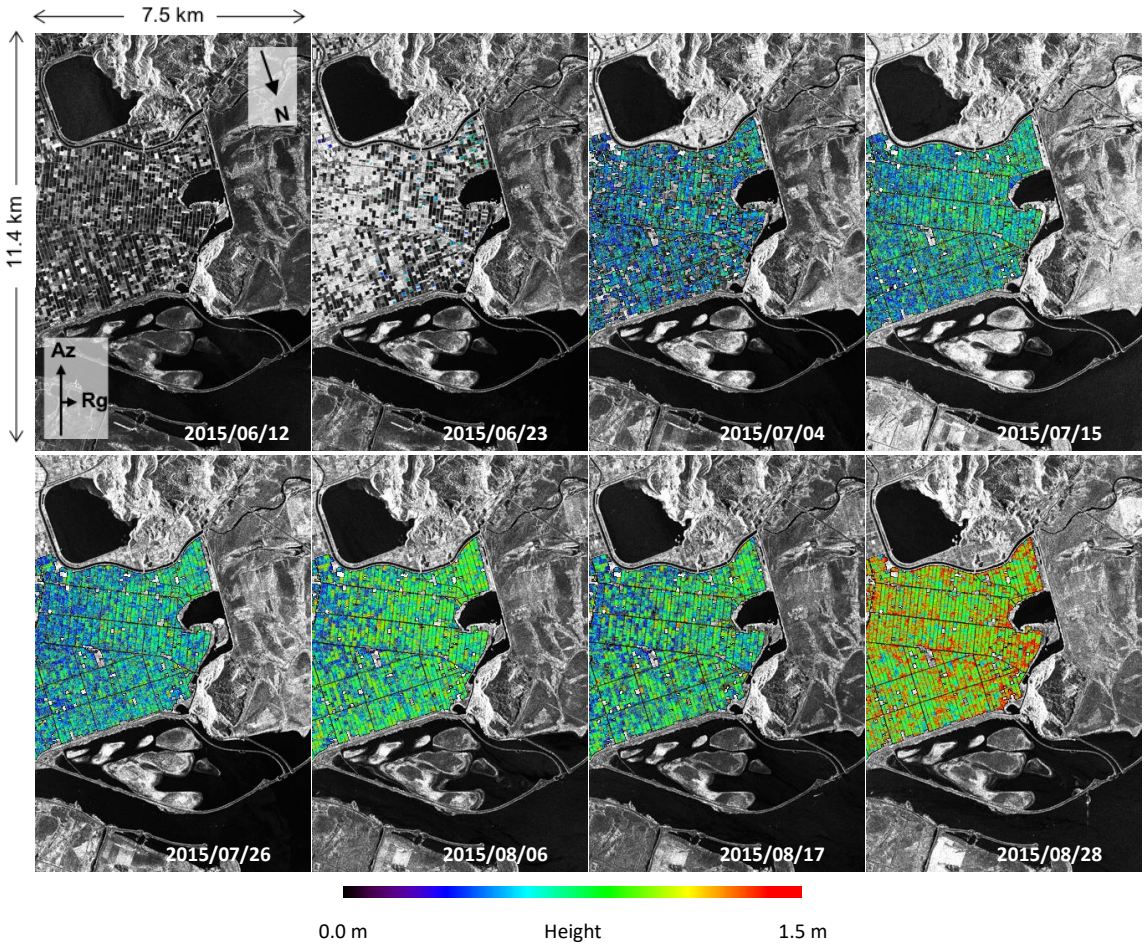

Figure 8. Temporal evolution of rice height changes from 23 June to 28 August 2015. The height maps are scaled from 0 m to 1.5 m. There is no height result for the first date. The first to third acquisitions are used for the water level estimate on a field-to-field basis.

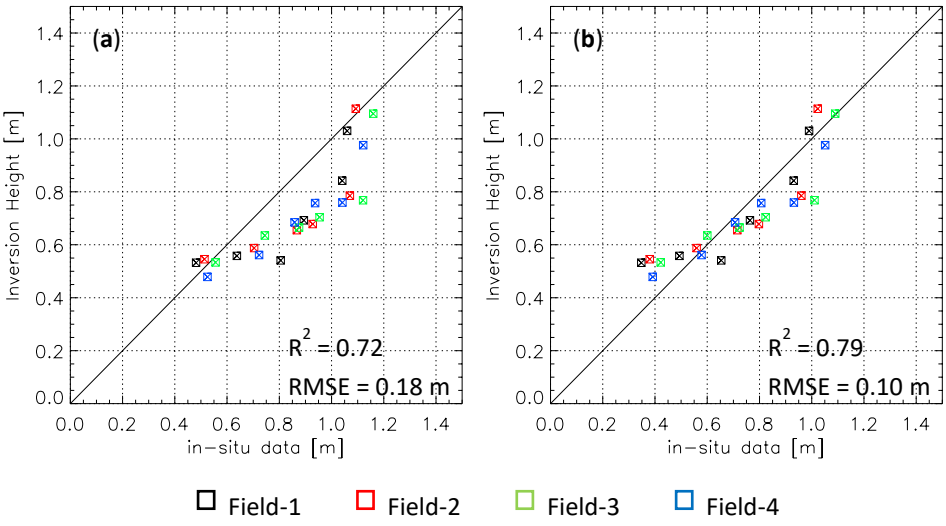

Figure 9. The comparison between inversion results and in-situ rice heights. (**a**) Root-to-top and (**b**) water surface to the top.

5. Conclusions

The retrieval of rice height within paddies was investigated and assessed using single-pol TDX datasets with large cross-track baselines. The single-pol TDX data used in this study can provide

a TDX image swath twice as large or at better spatial resolution, compared with a dual-pol dataset. In addition, against fully polarimetric TDX, the single-pol TDX data contains less SNR decorrelation.

In order to overcome the underdetermined problem in the model from the single polarization data, we attempted to estimate the ground (i.e., water level) phase from interferometric TDX datasets acquired immediately after the planting of the rice seedling. The primary limitation upon the water level estimate is that water management is controlled by field owners on a field-by-field basis. We were able to overcome this by measuring the water level elevation in paddies with a high coherence on a field-by-field basis with an assumption of flat topography for each parcel. The measured ground phase enabled the inversion model to be achieved using single-pol data for the retrieval of rice height above a water surface without the use of external topographical information.

The proposed single-pol inversion approach provided time-series height maps of rice paddy height. The inversion performance over rice fields was characterized by a correlation coefficient of 0.78 with the RMSE of 0.10 m, against the ground measurement. To accurately compare inversion height and field data, the water depth on the day of image acquisition must be known. We were able to account for this using available GIS information and confirmed that the water level decreased by approximately 10 cm with an increase in DoY. Without this compensation, a bias between the ground height and the model-based inversion height would have occurred.

These height map can be used to monitor the development of rice growth and assume the final production volume and rice yields. The proposed single-pol TDX approach can also be applied to other types of annual vegetation with non-flooded ground conditions, using an external DEM generated from a non-vegetated period.

Author Contributions: Data curation, S.-K.L. and S.Y.Y.; Formal analysis, S.-K.L.; Funding acquisition, J.-S.W.; Investigation, S.-K.L. and S.Y.Y.; Methodology, S.-K.L.; Project administration, J.-S.W.; Writing–original draft, S.-K.L.; Writing–review & editing, J.-S.W.

Funding: This research was funded by Global Surveillance Research Center (GSRC) program funded by the Defense Acquisition Program Administration (DAPA) and Agency for Defense Development (ADD), and in part by National Aeronautics and Space Administration (NASA) Carbon Monitoring System (CMS) program.

Acknowledgments: The author would like to thank TanDEM-X Science Coordination Team at DLR for TDX data and Nathan Thomas and Batuhan Osmanoglu at NASA/GSFC for their valuable comments to improve the quality of this paper. The author sincerely appreciate the National Institute of Agricultural Sciences (NAAS) for providing the in-situ data of rice height measured at the test site.

Conflicts of Interest: The authors declare no conflict of interest.

References

1. Rejesus, R.M.; Mohanty, S.; Balagtas, J.V. Forecasting Global Rice Consumption. 2012. Available online: http://www.agecon.purdue.edu/staff/balagtas/rice_timeseries_v6.pdf (accessed on 20 March 2012).
2. FAO. *A Regional Rice Strategy for Sustainable Food Security in Asia and the Pacific*; FAO: Rome, Italy, 2014; Available online: http://www.fao.org/3/a-i3643e.pdf (accessed on 26 October 2018).
3. Cloude, S.R.; Papathanassiou, K.P. Polarimetric SAR interferometry. *IEEE Trans. Geosci. Remote Sens.* **1998**, *36*, 1551–1565. [CrossRef]
4. Cloude, S.R. Dual-baseline coherence tomography. *IEEE Geosci. Remote Sens. Lett.* **2007**, *4*, 127–131. [CrossRef]
5. Cloude, S.R.; Papathanassiou, K.P. Three-stage inversion process for polarimetric SAR interferometry. *IEE Proc. Radar Sonar Navig.* **2003**, *150*, 125–134. [CrossRef]
6. Cloude, S.R. *Polarisation: Applications in Remote Sensing*; Oxford University Press: Oxford, UK, 2009.
7. Hajnsek, I.; Kugler, F.; Lee, S.-K.; Papathanassiou, K.P. Tropical-forest-parameter estimation by means of Pol-InSAR: The INDREX-II campaign. *IEEE Trans. Geosci. Remote Sens.* **2009**, *47*, 481–493. [CrossRef]
8. Lee, S.-K.; Kugler, F.; Papathanassiou, K.P.; Hajnsek, I. Quantification of temporal decorrelation effects at L-band for polarimetric SAR interferometry applications. *IEEE J. Sel. Top. Appl. Earth Obs. Remote Sens.* **2013**, *6*, 1351–1367. [CrossRef]

9. Kugler, F.; Lee, S.-K.; Hajnsek, I.; Papathanassiou, K.P. Forest height estimation by means of Pol-InSAR data inversion: The role of the vertical wavenumber. *IEEE Trans. Geosci. Remote Sens.* **2015**, *53*, 5294–5311. [CrossRef]
10. Parks, J.; Kugler, F.; Papathanassiou, P.; Hajnsek, I.; Hallikanien, M. Tree height estimation for boreal forest by means of L and X band PolInSAR and HUTCAT scatterometer. *IEEE Geosci. Remote Sens. Lett.* **2007**, *4*, 466–470. [CrossRef]
11. Lavalle, M.; Simard, M.; Hensly, S. A temporal decorrelation model for polarimetric radar interferometry. *IEEE Trans. Geosci. Remote Sens.* **2012**, *50*, 2880–2888. [CrossRef]
12. Simard, M.; Denbina, M. An assessment of temporal decorrelation compensation methods for forest canopy height estimation using airborne L-band same-day repeat-pass polarimetric SAR interferometry. *IEEE J. Sel. Top. Appl. Earth Obs. Remote Sens.* **2018**, *11*, 95–111. [CrossRef]
13. Kugler, F.; Schulze, D.; Hajnsek, I.; Pretzsch, H.; Papathanassiou, K.P. TanDEM-X Pol-InSAR performance for forest height estimation. *IEEE Trans. Geosci. Remote Sens.* **2014**, *52*, 6404–6422. [CrossRef]
14. Lee, S.-K.; Kugler, F.; Papathanassiou, K.; Hajnsek, I. Multibaseline polarimetric SAR interferometry forest height inversion approaches. In Proceedings of the 5th International Workshop POLinSAR, Frascati, Italy, 24–28 January 2011.
15. Lee, S.-K.; Fatoyinbo, T.E.; Lagomasino, D.; Feliciano, E.; Trettin, C. Multibaseline TanDEM-X Mangrove Height Estimation: The Selection of the Vertical Wavenumber. *IEEE J. Sel. Top. Appl. Earth Obs. Remote Sens.* **2018**, *8*, 3608–3618. [CrossRef]
16. Krieger, G.; Moreira, A.; Fiedler, H.; Hajnsek, I.; Werner, M.; Younis, M.; Zink, M. TanDEM-X: A satellite formation for high-resolution SAR interferometry. *IEEE Trans. Geosci. Remote Sens.* **2007**, *45*, 3317–3341. [CrossRef]
17. Zink, M.; Bachmann, M.; Bräutigam, B.; Fritz, T.; Hajnsek, I.; Moreira, A.; Wessel, B.; Krieger, G. TanDEM-X: The new global DEM takes shape. *IEEE J. Mag.* **2014**, *2*, 8–23. [CrossRef]
18. Zink, M.; Backmann, M.; Braeutigam, B.; Fritz, T.; Hajnsek, I.; Krieger, G.; Wessel, B. TanDEM-X Mission Status: The Complete Topography of the Earth. In Proceedings of the 2016 IEEE International Geoscience and Remote Sensing Symposium, Beijing, China, 10–15 July 2016; pp. 317–320.
19. TanDEM-X Ground Segment DEM Products Specification Document. TD-GS-PS-0021. 2016. Available online: https://tandemx-science.dlr.de/ (accessed on 5 August 2016).
20. Lee, S.-K.; Fatoyinbo, T.E. TanDEM-X Pol-InSAR inversion for mangrove canopy height estimation. *IEEE J. Sel. Top. Appl. Earth Obs. Remote Sens.* **2015**, *8*, 3608–3618. [CrossRef]
21. Sadeghi, Y.; St-Onge, B.; Leblon, B.; Simard, M. Canopy height model (CHM) derived from a TanDEM-X InSAR DSM and an airborne lidar DTM in boreal forest. *IEEE J. Sel. Top. Appl. Earth Obs. Remote Sens.* **2016**, *9*, 381–397. [CrossRef]
22. Soja, M.J.; Askne, J.I.H.; Ulander, L.M.H. Estimation of boreal forest properties from TanDEM-X data using inversion of the interferometric water cloud model. *IEEE Geosci. Remote Sens. Lett.* **2017**, *14*, 997–1001. [CrossRef]
23. Soja, M.J.; Persson, H.J.; Ulander, L.M.H. Estimation of forest biomass from two-level model inversion of single-pass InSAR data. *IEEE Geosci. Remote Sens. Lett.* **2015**, *53*, 5083–5099. [CrossRef]
24. Treuhaft, R.; Goncalves, F.; dos Santos, J.R.; Keller, M.; Palace, M.; Madsen, S.N.; Sullivan, F.; De Alencastro Graça, P. Tropical-forest biomass estimation at X-band from the spaceborne TanDEM-X interferometer. *IEEE Geosci. Remote Sens. Lett.* **2015**, *12*, 239–243. [CrossRef]
25. Rossi, C.; Erten, E. Paddy-rice monitoring using TanDEM-X. *IEEE Trans. Geosci. Remote Sens.* **2015**, *53*, 900–910. [CrossRef]
26. Hajnsek, I.; Busche, T. TanDEM-X: Science activities. In Proceedings of the 2015 IEEE International Geoscience and Remote Sensing Symposium, Milan, Italy, 26–31 July 2015; pp. 2892–2894.
27. Announcement of Opportunity: TanDEM-X Science Phase, TD-PD-PL-0032. 2014. Available online: https://tandemx-science.dlr.de/ (accessed on 19 May 2014).
28. Erten, E.; Lopez-Sanchez, J.M.; Yuzugullu, O.; Hajnsek, I. Retrieval of agricultural crop height from space: A comparison of SAR techniques. *Remote Sens. Environ.* **2016**, *187*, 130–144. [CrossRef]
29. Lopez-Sanchez, J.M.; Vicente-Guijalba, F.; Erten, E.; Campos-Taberner, M.; Garcia-Haro, F.J. Retrieval of vegetation height in rice fields using polarimetric SAR interferometry with TanDEM-X. *Remote Sens. Environ.* **2017**, *192*, 33–44. [CrossRef]

30. Yuzugullu, O.; Erten, E.; Hajnsek, I. Assessment of Paddy Rice Height: Sequential Inversion of Coherent and Incoherent Models. *IEEE J. Sel. Top. Appl. Earth Obs. Remote Sens.* **2018**, *11*, 3001–3013. [CrossRef]
31. TerraSAR-X Basic Product Specification, TX-GS-DD-3302. 2009. Available online: http://sss.terrasar-x.dlr.de/ (accessed on 26 October 2018).
32. Yoon, S.Y.; Lee, S.-K.; Won, J.-S. Rice Paddy Height Estimation from Single-polarization TanDEM-X Science Phase Data. In Proceedings of the 2017 IEEE International Geoscience and Remote Sensing Symposium, Fort Worth, TX, USA, 23–28 July 2017; pp. 930–933.
33. TanDEM-X Payload Ground Segment: CoSSC Generation and Interferometric Consideration. TP-PGS-TN-3129. 2012. Available online: https://tandemx-science.dlr.de/ (accessed on 15 May 2012).
34. Gatelli, F.; Monti Guarnieri, A.; Parizzi, F.; Pasquali, P.; Prati, C.; Rocca, F. The wavenumber shift in SAR interferometry. *IEEE Trans. Geosci. Remote Sens.* **1994**, *32*, 855–864. [CrossRef]
35. Lee, S.-K.; Ryu, J.-H. High-accuracy tidal flat digital elevation model construction using TanDEM-X Science Phase data. *IEEE J. Sel. Top. Appl. Earth Obs. Remote Sens.* **2017**, *10*, 2713–2724. [CrossRef]
36. Statistics Korea, Agricultural Area Investigation. 2015. Available online: http://meta.narastat.kr/metasvc/svc/SvcMetaDcDtaPopup.do?orgId=101&confmNo=114033&kosisYn=Y (accessed on 26 October 2018).
37. Yuzugullu, O.; Erten, E.; Hajnsek, I. Rice growth monitoring by means of X-band co-polar SAR: Feature clustering and BBCH scale. *IEEE Geosci. Remote Sens. Lett.* **2015**, *12*, 1218–1222. [CrossRef]
38. Ballester-Berman, J.D.; Lopez-Sanchez, J.M. Combination of direct and double-bounce ground responses in the homogeneous oriented volume over ground model. *IEEE Geosci Remote Sens. Lett.* **2011**, *8*, 54–58. [CrossRef]
39. Ballester-Berman, J.D.; Lopez-Sanchez, J.M.; Fortuny-Guasch, J. Retrieval of biophysical parameters of agricultural crops using polarimetric SAR interferometry. *IEEE Trans. Geosci. Remote Sens.* **2005**, *43*, 683–694. [CrossRef]
40. Erten, E.; Rossi, C.; Yuzugullu, O. Polarization impact in TanDEM-X data over vertical-oriented vegetation: The paddy-rice case study. *IEEE Geosci. Remote Sens. Lett.* **2015**, *12*, 1501–1505. [CrossRef]
41. Lopez-Sanchez, J.M.; Ballester-Berman, J.D.; Hajnsek, I. First results of rice monitoring practices in Spain by means of time series of TerraSAR-X dual-pol images. *IEEE J. Sel. Top. Appl. Earth Obs. Remote Sens.* **2011**, *4*, 412–422. [CrossRef]
42. Lopez-Sanchez, J.M.; Ballester-Berman, J.D.; Marquez-Moreno, Y. Model limitations and parameter estimation methods for agricultural applications of polarimetric SAR interferometry. *IEEE Trans. Geosci. Remote Sens.* **2007**, *45*, 3481–3493. [CrossRef]
43. Lopez-Sanchez, J.M.; Cloude, S.R.; Ballester-Berman, J.D. Rice phenology monitoring by means of SAR polarimetry at X-band. *IEEE Trans. Geosci. Remote Sens.* **2012**, *50*, 2695–2709. [CrossRef]
44. Lopez-Sanchez, J.M.; Vicente-Guijalba, F.; Ballester-Berman, J.D.; Cloude, S.R. Influence of incidence angle on the coherent copolar polarimetric response of rice at X-band. *IEEE Geosci. Remote Sens. Lett.* **2015**, *12*, 249–253. [CrossRef]
45. Kim, S.-W.; Hong, S.-H.; Won, J.-S. An Application of L-band Synthetic Aperture Radar to Tide height Measurement. *IEEE Trans. Geosci. Remote Sens.* **2005**, *43*, 1472–1478.
46. Lee, S.-K.; Hong, S.-H.; Kim, S.-W.; Yamaguchi, Y.; Won, J.-S. Polarimetric Features of Oyster Farm Observed by AIRSAR and JERS-1. *IEEE Trans. Geosci. Remote Sens.* **2005**, *44*, 2728–2735. [CrossRef]
47. *Radiometric Calibration of TerraSAR-X Data: Beta Naught and Sigma Naught Coefficient Calculation*; INFOTERRA: Friedrichshafen, Germany, 2008.